Characterization and deactivation studies of an activated sulfided red mud used as hydrogenation catalyst

Jorge Alvarez, Roberto Rosal, Herminio Sastre, Fernando V. Díez[*]

Department of Chemical and Environmental Engineering, University of Oviedo, 33071-Oviedo, Spain

Abstract

Red mud is a residue in the production of alumina by the Bayer process that contains oxides of Fe and Ti, active as hydrogenation catalyst in sulfided form, and whose catalytic activity can be improved by the activation method proposed by Pratt and Christoverson. The development of its activity and selectivity with reaction time was studied for the hydrogenation of a light fraction of an anthracene oil, and compared with untreated sulfided red mud. Catalyst samples were collected at different reaction times, and their texture, morphology and composition characterized by nitrogen adsorption, SEM and SEM–EDX. The loss of catalytic activity of activated sulfided red mud is slower than for untreated sulfided red mud. The main cause of this decrease in catalytic activity is the loss of surface area and superficial Fe. © 1998 Elsevier Science B.V.

1. Introduction

Red mud is a by-product in the manufacture of alumina by the Bayer process, that contains mainly oxides of iron, aluminium, titanium, silicon, calcium and sodium. Sulfided red mud is active as hydrogenation catalyst, due to its iron sulfide content, and has been used for the hydrogenation of organic compounds [1,2], and the liquefaction of coal [2–4] and biomass [5].

In previous work, sulfided red mud has been tested as a catalyst for the hydrogenation of anthracene oil (a fraction obtained by distillation of coal tar, containing two- to four-ring condensed aromatic hydrocarbons)

[6], and its deactivation for this reaction has also been studied [7]. Catalytic hydrogenation of anthracene oil yields a solvent with high hydrogen-donor capacity, due to its content in hydroaromatic compounds such as dihydroanthracene, dihydrophenanthrene and tetrahydrofluoranthene. Hydrogenated anthracene oil can be used in processes in which transferable hydrogen plays an important role, such as coal liquefaction [8,9], oil–coal coprocessing [10], and coke production by carbonization of low-rank coals with pitch-like materials [11].

The previously mentioned studies of the development with time of the red mud activity were carried out at constant temperature (623 K), pressure (10 MPa) and flow rates (hydrogen 4×10^{-6} Nm^3/s, liquid feed 0.6 ml/min, at room conditions). Catalyst samples were collected after different reaction times

*Corresponding author. Tel.: +34-8-5103508; Fax: +34-8-5103434; E-mail: fds@dwarf1.quimica.uniovi.es

and characterized by BET nitrogen adsorption, scanning electron microscopy (SEM), and SEM–EDX. It was found that sulfided red mud lost its catalytic activity after 40 h reaction time. The loss of catalytic activity was explained by the loss of BET surface area (45% lost in the 40 h period), combined with the progressive loss of superficial iron, measured by EDX maps (74% loss in the 40 h period).

Several methods have been proposed for enhancing the red mud catalytic activity. Pratt and Christoverson [1] proposed a dissolution–precipitation method, which decreases the Ca and Na content (Na is known to enhance sintering [12]), and increases its specific surface. Red mud modified by the method of Pratt and Christoverson will be referred to in this work as "activated red mud". Sulfided activated red mud was tested as a catalyst for the hydrogenation of anthracene oil [6], and was found to be more active than untreated sulfided red mud for the hydrogenation of acenaphthene, anthracene, phenanthrene, fluoranthene and pyrene.

In the present work, the development with time of the catalytic activity and selectivity of a sulfided red mud activated by the method of Pratt and Christoverson for the hydrogenation of anthracene oil was studied. Reactions were carried out at constant temperature, pressure and flow rates. Catalyst samples were collected after different reaction times and characterized by BET nitrogen adsorption, scanning electron microscopy (SEM), and SEM–EDX. The catalytic performance of the activated red mud was compared with the non-activated red mud.

2. Experimental

2.1. Materials

The red mud used in this work was supplied by the San Ciprián (Lugo, Spain) plant of the Spanish aluminium company Inespal. It was analyzed by atomic absorption spectrometry and volumetric methods after acid dissolution and alkaline fusion. Its composition is given in Table 1, and details of the analytical method are given in [13]. The red mud was activated by the method of Pratt and Christoverson [1], which essentially consists in dissolving the red mud in aqueous HCl, boiling the resulting solution for 2 h, and adding

Table 1
Bulk and EDX composition of red mud and activated red mud

Element	Red mud (wt.%)		Activated red mud (wt.%)	
	Bulk	EDX	Bulk	EDX
Fe	19.7	21.7	25.1	28.9
Ti	13.0	11.9	16.1	12.8
Al	7.9	7.4	9.0	7.9
Na	3.7	3.0	0.1	0.4
Ca	5.1	4.9	0.9	4.1
Si	4.7	3.6	4.9	2.7
P	0.1	0.7	0.2	0.7
V	n.m.	0.3	n.m.	0.3
Cl	n.m.	0.3	n.m.	>0.1

Table 2
Composition of anthracene oil (wt.%)

Naphthalene	4.0
Acenaphthene	5.9
Dibenzofuran	3.1
Fluorene	4.9
9,10-Dihydroanthracene	0.8
Phenanthrene	18.2
Anthracene	4.4
Carbazole	2.9
Fluoranthene	10.2
Pyrene	6.2
2-Methylnaphthalene	1.0
Dibenzothiophen	1.2
Methylanthracene	1.1
Methylphenanthrene	1.2
Methylpyrene	1.5
Chrysene	1.7
Triphenilene	1.8

aqueous ammonia until pH=8. The resulting precipitate is filtered, washed with distilled water, dried at 383 K, and calcined in air at 773 K for 2 h.

Reaction studies were carried out by hydrogenating a light fraction of anthracene oil supplied by Nalon-Chem (Asturias, Spain); its composition is given in Table 2.

2.2. Catalyst characterization

Catalyst morphology and superficial composition were studied by SEM–EDX in a JSM-6100 apparatus equipped with a Link X-ray microanalizer. Catalyst samples must be gold-coated for morphological examination, and polished and carbon-coated for EDX studies. EDX provides a quantitative chemical

analysis of a catalyst surface layer to a depth of about 1 micron, and supplies maps of the distribution of certain elements.

Catalyst pore structure and surface area were measured by nitrogen adsorption with a Micromeritics Asap 2000 apparatus.

X-ray diffraction studies were carried out in a Siemens D 5000 Dust Diffractometer, provided with monochromator and sparkling detector.

Each used catalyst sample was Soxhlet extracted with toluene for 48 h, and dried at 383 K for 12 h, prior to its characterization.

2.3. Reaction studies

The reactor used for the hydrogenation experiments was a 9 mm internal diameter, 45 cm long stainless steel cylinder. 2.0 g of activated red mud were placed in the central section of the reactor, the upper and lower sections being filled with low-area inert alumina. The red mud was sulfided in situ before use by passing a mixture of 10% hydrogen sulfide in hydrogen at atmospheric pressure, heated to 673 K, through the reactor for 4 h. 1 wt.% carbon sulphide was added to the liquid feed to maintain the catalyst in the sulfided form. The reactor was operated as a continuous trickle bed reactor, liquid and gas feeds flowing cocurrently downwards. The liquid feed consisted of 20 wt.% anthracene oil dissolved in toluene for easier handling, and the gas feed consisted of high pressure hydrogen. Hydrogenated anthracene oil was analyzed by gas chromatography using a capillary fused silica column with apolar stationary phase SE-30, and peak assignment was performed by gas chromatography-mass spectrometry. Reactions were carried out under the same conditions as the experiments using untreated red mud [7], mentioned in Section 1 of this work. Further details of the reaction experimental set up and procedure are given elsewhere [6].

3. Results and discussion

3.1. Catalysts characterization

Red mud and activated red mud bulk compositions, determined by classical chemical analysis, along with the surface composition, measured by EDX, are given in Table 1. Textural characteristics, obtained by nitrogen adsorption, are given in Table 3. It can be observed that the activation method is efficient in reducing the red mud Na and Ca content, and in increasing its specific surface and pore volume.

X-ray diffractograms are given in Fig. 1. The constituents identified by X-ray diffraction are: Rutile (TiO_2), Hematite (Fe_2O_3), Goethite and Lepidocrocite (FeO(OH)), Iron Hydroxide (Fe(OH)$_3$), Halloysite ($Al_2Si_2O_5(OH)_4$) and Bayerite (Al(OH)$_3$). The activation method of Pratt and Christoverson eliminates the aluminium-containing crystalline forms, Bayerite and Halloysite, which are substituted by amorphous forms, since the activation method does not decrease the aluminium content. The iron-containing crystalline components Lepidocrocite and Iron Hydroxide also disappear after activation, probably due to the calcination step. The effect of sulfidation for both untreated and activated red mud is decreasing the content of the crystalline iron oxides and hydroxides, which are transformed into Pyrrothyte ($Fe_{(x-1)}S_x$). Halloysite is also removed from untreated red mud by sulfidation.

3.2. Catalyst deactivation

Among the anthracene oil constituents, only anthracene, phenanthrene, fluoranthene, and pyrene were found to be measurably hydrogenated under reaction conditions. Their main hydrogenated products were 9,10-dihydroanthracene, 9,10-dihydrophenanthrene, 1,2,3,10b-tetrahydrofluoranthene and 4,5-dihydro-

Table 3
Textural characteristics of different red mud samples, obtained by nitrogen adsorption

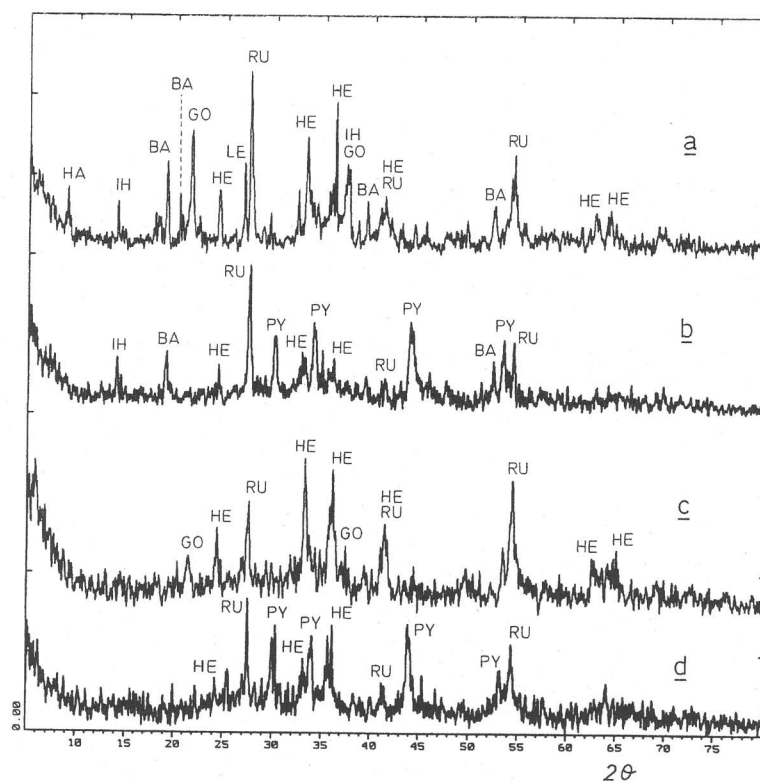|	Red mud		Activated red mud		After reaction time			
	Unsulfided	Sulfided	Unsulfided	Sulfided	1 h	3 h	12 h	68 h
BET specific surface (m^2/g)	24.3	29.5	82.4	85.4	58.9	48.8	49.3	48.1
BJH desorption pore volume, (cm^3/g)	0.086	0.090	0.227	0.170	0.152	0.083	0.108	0.113
BET average pore diameter, (nm)	12.1	10.5	9.8	8.6	9.6	7.4	8.7	9.3

Fig. 1. X-ray diffractograms for: (a) untreated red mud, (b) sulfided untreated red mud, (c) activated red mud, (d) sulfided activated red mud. BA, bayerite; GO, goethite; HA, halloysite; HE, hematite; IH, iron hydroxide; LE, lepidocrocite; PY, pyrrothyte; RU, rutile.

pyrene, respectively. The compounds hydrogenated and their hydrogenation products are the same as when sulfided untreated red mud is used as catalyst. It has been shown [14] that hydrogenation of these compounds accounts for more than 75% of the total hydrogen consumption. The evolution of the conversion of the different compounds with reaction time is shown in Fig. 2. After an initial period of about 6 h of fast catalytic activity decay, conversions remain almost constant for a period of approx. 47 h. During the next 20 h, conversions decay again sharply, so that at 70 h reaction time the only reactant converted was anthracene. The effectiveness of Pratt and Christoverson's activation method for increasing both the red mud activity and resistance to deactivation is apparent in Fig. 3, in which the changes of the average conversion with time for untreated and activated red mud are compared. Average conversion is defined as:

average conversion

$$= \frac{\Sigma \text{ compounds in feed} - \Sigma \text{ compounds in product}}{\Sigma \text{ compounds in feed}}$$

where Σ compounds is the sum of the concentrations of anthracene, phenanthrene, fluoranthene and pyrene.

In different experiments, catalyst samples were collected after 3, 12 and 68 h reaction time, the last sample corresponding to the almost completely deactivated catalyst.

The development of textural properties of sulfided activated red mud with reaction time can be observed in Table 3 and Fig. 4. The surface area decreased during the first 3 h of reaction time to 57%, subsequently remaining almost unchanged.

SEM photographs of the sulfided catalyst, fresh and after 68 h reaction time are shown in Figs. 5 and 6. After 68 h reaction time, the catalyst seems to be made up of large particles whose surface is rather flat,
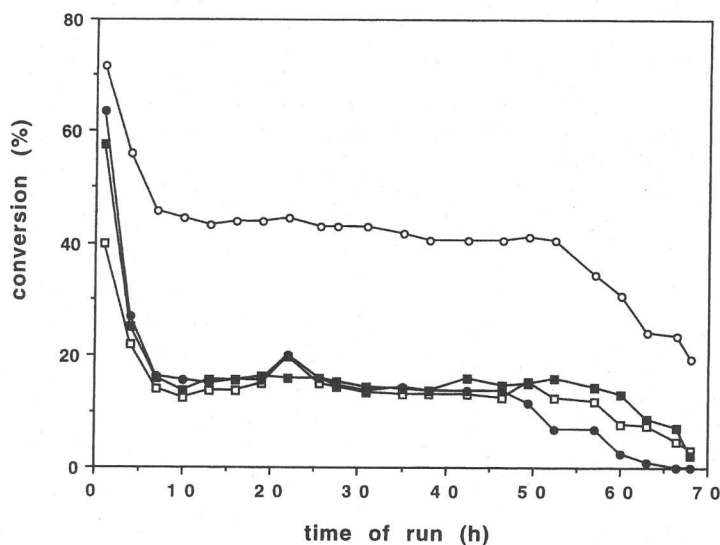
Fig. 2. Conversions versus run time for: ○ anthracene, □ phenanthrene, ■ fluoranthene, ● pyrene.
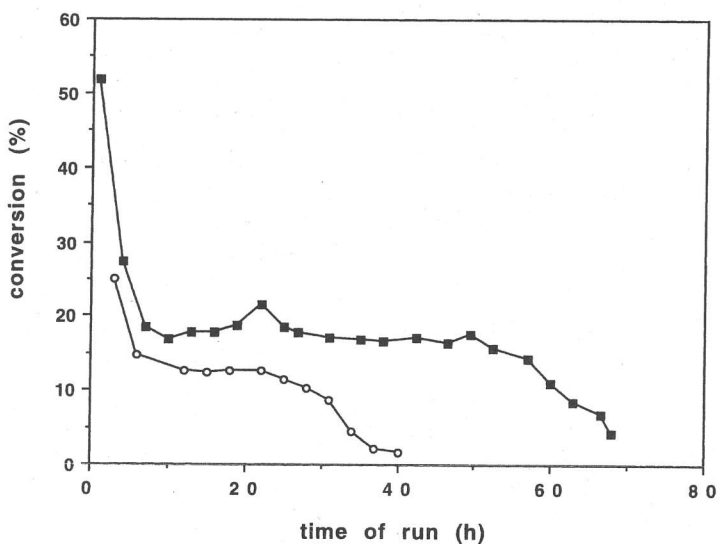

Fig. 3. Average conversions versus run time for: ○ sulfided untreated red mud, ■ sulfided activated red mud.

alongside granular zones similar in aspect to the fresh catalyst. The two different zones that appear in the used catalyst were characterized by SEM–EDX, pointing the X-ray beam adequately. The resulting spectra, shown in Fig. 7, show that the flat-surfaced big particles are mainly made up of alumina, while the small granules are mainly formed by iron sulfide.

SEM–EDX concentrations of the different activated red mud samples are given in Table 4. A sharp increase in aluminium, and a decrease in iron and calcium concentrations as the reaction proceeds can be observed.

Figs. 8–10 show EDX maps of the distribution of certain elements in the catalyst samples. The bright-
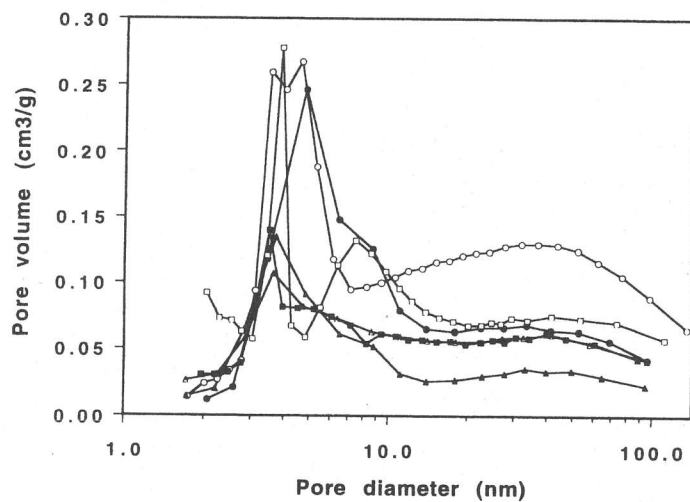
Fig. 4. Pore volume distributions of the activated red mud: ○ fresh, unsulfided; ● fresh, sulfided; ▲ after 1 h; □ after 3 h; ■ after 12 h; △ after 68 h.
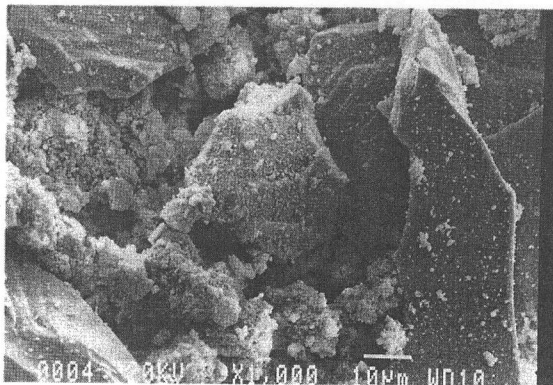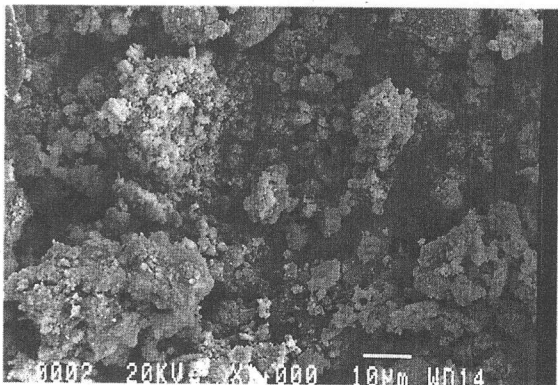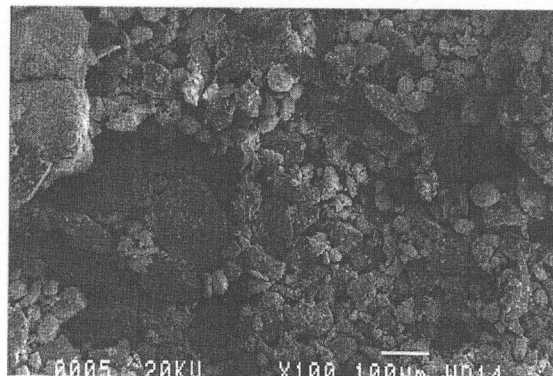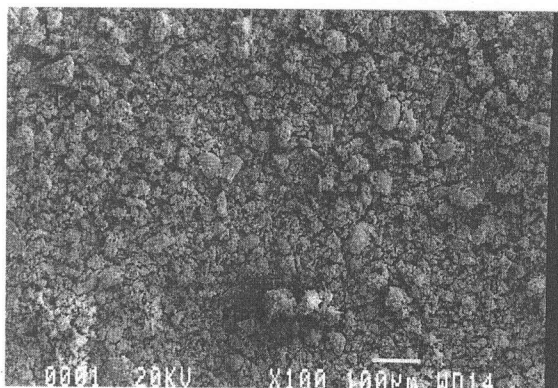

Fig. 5. SEM photographs of the surface of fresh sulfided activated red mud at different magnifications.

Fig. 6. SEM photographs of the surface of sulfided activated red mud after 68 h run time at different magnifications.
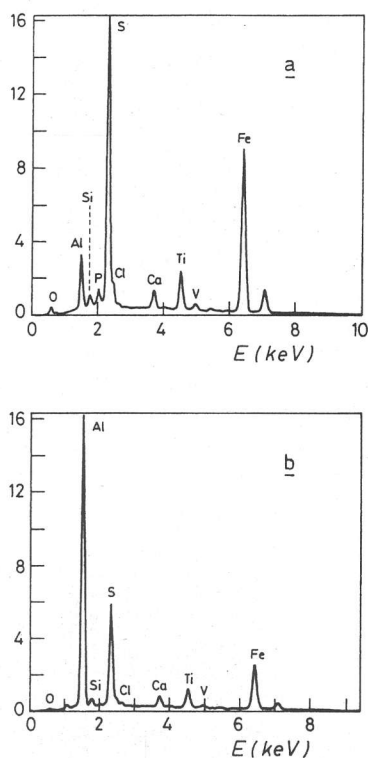
Fig. 7. SEM–EDX spectra corresponding to different zones of used sulfided activated red mud: (a) zone formed by small granules, (b) zone formed by big, flat-surfaced particles.

Fig. 8. SEM–EDX maps of distribution of elements of fresh, sulfided activated red mud.

Table 4
EDX composition of sulfided activated red mud after different reaction times in the presence of H_2S (wt.%)

Element	Reaction time				
	0 h	1 h	3 h	12 h	68 h
Fe	41.0	36.2	39.8	34.4	33.1
Ti	15.2	15.5	13.8	16.1	15.4
S	19.8	13.3	19.5	17.1	17.4
Al	14.9	19.8	15.8	21.0	24.4
Ca	4.0	3.6	2.6	5.3	2.0
Si	3.9	9.7	6.2	2.9	4.3
Na	4.0	3.6	2.6	5.3	2.9
Cl	0.0	0.0	0.0	0.7	0.6
P	0.0	0.7	0.8	0.6	0.9
V	0.4	0.5	0.4	0.4	0.2

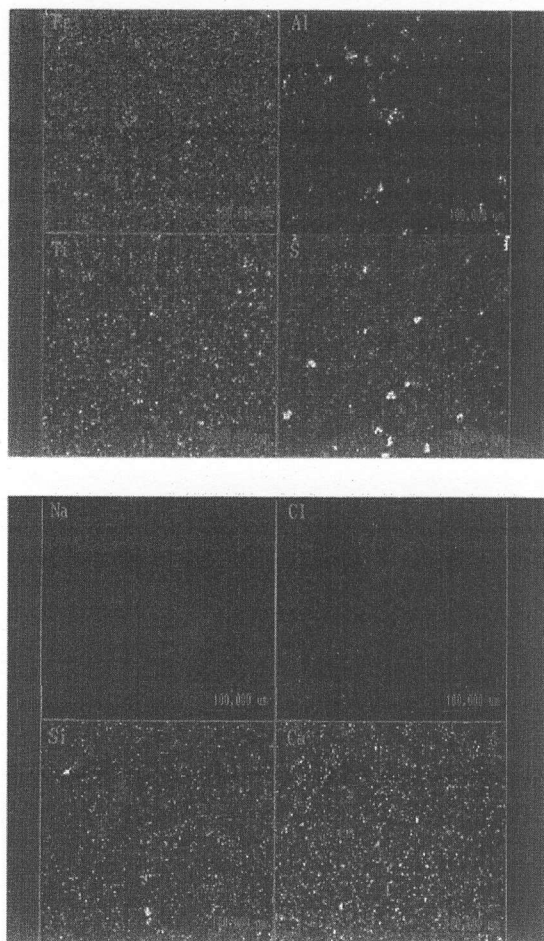ness of every pixel in these maps is related to the intensity of emission of the characteristic k_α line of each element, and thus to its concentration in the surface layer, white corresponding to a high concentration of a given element, black to the absence of this element, and greys to intermediate concentrations. The pictures corresponding to the elements at high concentrations (iron, aluminium, titanium and sulfur) were obtained by setting a different level of brightness to the ones corresponding to the elements at low concentrations (sodium, chlorine, silicon and calcium). The progressive occupation of the catalyst surface by aluminum to the detriment of iron, and the association of titanium, sulfur, silicium and calcium with iron can be observed. This corresponds to the progressive occupation of the catalyst surface by the big, flat, aluminium-containing particles observed by SEM.
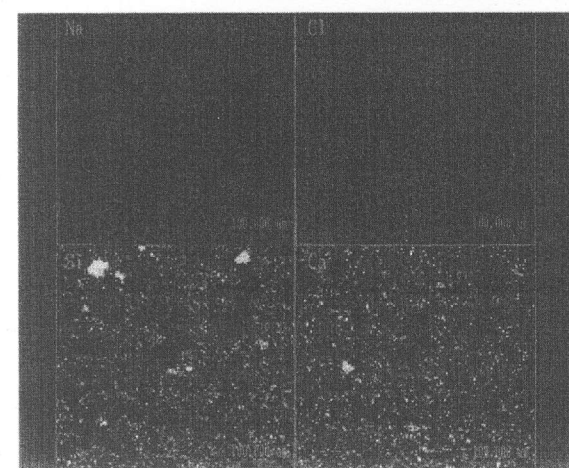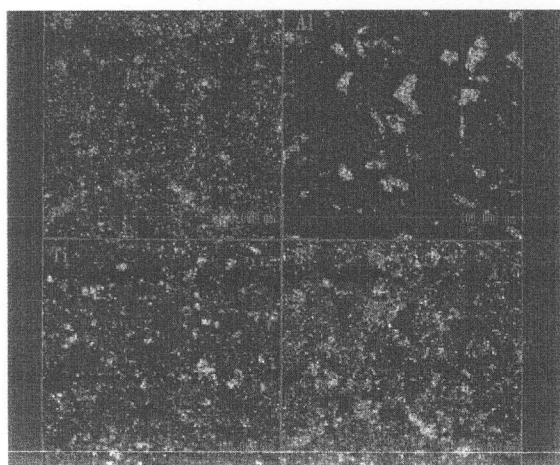
Fig. 9. SEM–EDX maps of distribution of elements of sulfided activated red mud after 12 h reaction time.
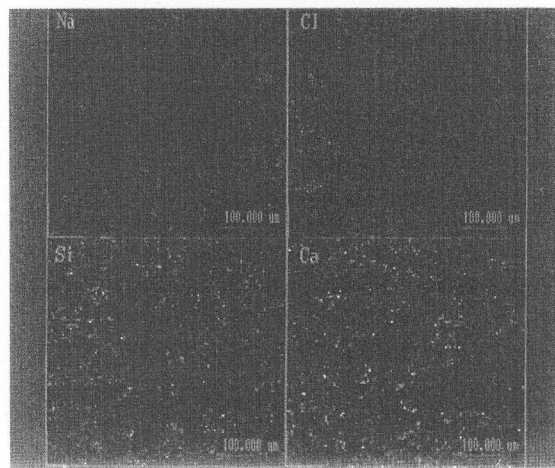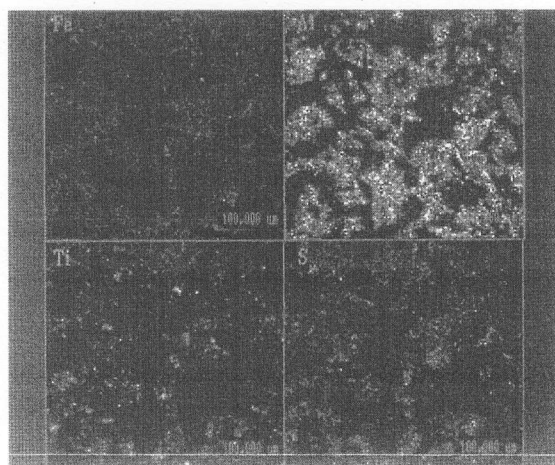

Fig. 10. SEM–EDX maps of distribution of elements of sulfided activated red mud after 68 h reaction time.

Taking into account the fact that the brightness of every pixel of the EDX maps, B, can be quantified on a scale of 0 (black) to 1 (maximum degree of brightness), $\Sigma B_i S_i$ (S_i being the surface fraction corresponding to a brightness B_i) can be taken as an alternative measure of the iron content in the 1 micron surface layer. According to this method, and taking 1 as the iron content of the fresh sulfided activated red mud, the catalyst iron content decreases to 0.98 after 3 h run time, 0.64 after 12 h run time, and 0.23 after 68 h run time. This decrease is much more pronounced than that given by the SEM–EDX data of Table 4.

The observed trend of both BET surface area and Fe surface content to decrease as the reaction proceeds is

similar to the behaviour observed for untreated red mud [7]. The morphological changes observed by SEM are also similar for both untreated and activated red mud. Comparison of activated red mud SEM–EDX maps with those corresponding to untreated red mud show a higher Ca and Al content for fresh sulfided red mud than for fresh sulfided activated red mud, and a faster increase in iron and decrease in aluminium content in the catalyst 1 micron surface layer for untreated red mud.

Fig. 11 shows the evolution with reaction time of the catalytic activity, relative to the activity of sulfided activated red mud after 3 h reaction time, for both untreated and activated red mud. Catalytic activity,
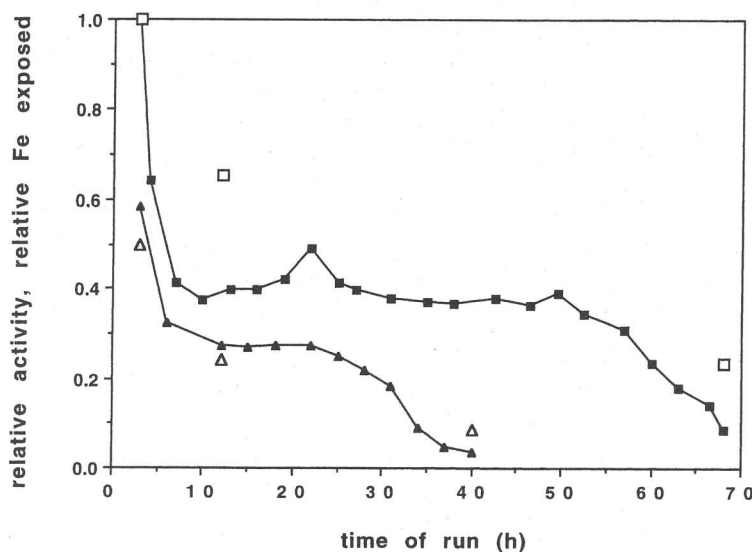
Fig. 11. Relative catalytic activity (▲ untreated red mud, ■ activated red mud) and relative iron content (△ untreated red mud, □ activated red mud) versus reaction time.

defined as the reaction rate under given conditions divided by the reaction rate under the reference conditions, is calculated by assuming first-order kinetics for the hydrogenation reactions [15]. Data of relative catalyst iron content, defined as the product of the surface area and iron content measured from the EDX maps, relative to the sulfided activated red mud after 3 h reaction time, are also plotted in the same figure. It can be observed that the catalytic activity for both untreated and activated red mud roughly correlates with the changes in iron content, assumed to be the active catalytic phase as iron sulfide, caused by the combination of the decrease in surface area and Fe surface content.

References

[1] K.C. Pratt, V. Christoverson, Fuel 61 (1982) 460.
[2] A. Eamsiri, R. Jackson, K.C. Pratt, V. Christov, M. Marshall, Fuel 71 (1992) 449.
[3] D. Garg, E.N. Givens, Ind. Eng. Chem. Process Des. Dev. 24 (1985) 66.
[4] S. Sato, M. Morita, T. Hashimoto, I. Mitunori, K. Chiba, H. Tagaya, Fuel 68 (1989) 622.
[5] B. Klopties, W. Hodek, F. Bandermann, Fuel 69 (1990) 448.
[6] J.J. Llano, R. Rosal, H. Sastre, F.V. Díez, Fuel 73 (1994) 688.
[7] J. Alvarez, R. Rosal, H. Sastre, F.V. Díez, Applied Catalysis A: General 128 (1995) 259.
[8] D.D. Whitehurst, T.O. Mitchell, M. Farcasiu, Coal Liquefaction, Academic Press, New York, 1980.
[9] K. Chiba, H. Tagoya, T. Kobayashi, Y. Shibuya, Ind. Eng. Chem. Res. 26 (1987) 1329.
[10] S.E. Moschopedis, J.G. Hawkins, J.F. Fryer, J.G. Speight, Fuel 59 (1980) 647.
[11] T. Yotono, H. Marsh, in: H.D. Schultz (Ed.), Coal Liquefaction Products: NMR Spectroscopic Characterization and Production Processes, Wiley, New York, 1983, p. 125.
[12] C.N. Satterfield, Heterogeneous Catalysis in Industrial Practice, 2nd ed., McGraw-Hill, 1991.
[13] J.J. Alvarez Rodríguez, M.Sc. Dissertation, University of Oviedo, 1994.
[14] R. Rosal, F.V. Díez, H. Sastre, Fuel 71 (1992) 761.
[15] R. Rosal, F.V. Díez, H. Sastre, Ind. Eng. Chem. Res. 31 (1992) 1007.